Mechanisms and Epitaxial Relationships between Close-Packed and BCC Lattices in Block Copolymer Solutions

Joona Bang[†] and Timothy P. Lodge*,[†,‡]

Department of Chemical Engineering and Materials Science and Department of Chemistry, University of Minnesota, Minneapolis, Minnesota 55455-0431

The epitaxial relationships between two close-packed lattices (face-centered cubic (fcc) and hexagonally close packed (hcp)) and the body-centered cubic (bcc) lattice of spherical micelles were investigated by small-angle X-ray scattering (SAXS) in two in situ shear cells. Two symmetric poly(styrene-*b*-isoprene) diblock copolymers with block molecular weights of 8.0×10^3 and 7.0×10^3 g/mol, and 1.5×10^4 and 1.5×10^4 g/mol, respectively, were employed. Thermoreversible fcc → bcc order−order transitions were identified in three styrene-selective solvents, dimethyl phthalate, diethyl phthalate and dibutyl phthalate, and in two isoprene-selective solvents, tetradecane and squalane. Upon shearing an fcc solution, a mixture of highly oriented fcc and hcp crystals was produced, due to the random stacking of the {111} planes along the shear gradient. A bcc phase was grown epitaxially from each hcp/fcc mixture by heating to a temperature within the bcc window without shear. By employing two shear cells, access to scattering along both the gradient axis and the vorticity axis was achieved. This proved crucial to elucidating both the fcc → bcc and hcp → bcc transformations. These mechanisms are related to the Bain distortion and the Burgers mechanism, respectively, which are well-established in simple metals. Interestingly, the close-packed planes in fcc/hcp ({111}$_{fcc}$ and {0002}$_{hcp}$ planes) and bcc ({110} planes) were preserved during these transformations, but bcc unit cells with nine distinct orientations were produced. These reflect particular orientation relationships (ORs) between the parent fcc/hcp and the newly formed bcc crystals, which correspond to the Kurdjumov-Sachs, Burgers, Nishiyama-Wassermann, and Pitsche-Schrader ORs that are prevalent in metals.

Introduction

The self-assembly characteristics of block copolymers lead to a rich variety of morphologies.[1,2] For diblock copolymers in the melt, the established equilibrium morphologies are lamellae (L), the gyroid (G), hexagonally packed cylinders (C), and a body centered cubic (bcc) array of spheres (S). In the vicinity of the order−disorder transition (ODT), block copolymers may exhibit thermoreversible order−order transitions (OOTs) between different morphologies. Many experimental studies have reported such OOTs, and their epitaxial relationships have been established,[3−10] even though the detailed kinetics and pathways are not yet fully understood. To investigate the transition mechanism in detail, small angle scattering with an in situ shear cell is the most powerful tool. Under appropriate shearing conditions, the initial phase is refined and oriented, giving rise to characteristic Bragg diffraction spots. By monitoring the changes in the diffraction patterns during the OOT, it is possible to identify the mechanism of the transition.

In block copolymer solutions, the phase behavior can be greatly affected by the solvent selectivity. We have recently mapped out in detail the phase behavior of poly(styrene-*b*-isoprene) (SI) diblock copolymers in a series of solvents of varying selectivity.[11−19] The temperature dependence of the solvent selectivity can induce several thermoreversible OOTs for a single polymer, depending on concentration (ϕ) and the composition of the copolymer (*f*). These include L → G, G → L, G → C, C → G, C → S, and S → C upon heating. At moderate concentrations, the block copolymers form spherical micelles. In contrast to the melt case, these micelles pack onto either a bcc or a face-centered cubic (fcc) lattice, depending on *f* and temperature. Furthermore, in many cases there is an fcc → bcc transition upon heating. We have presented a preliminary report of the epitaxial relationship associated with this transition,[20] and here we provide a full description of a rather complicated phenomenon. In particular, we demonstrate that the transition is observed for symmetric copolymers in both PS-selective and PI-selective solvents.

The pioneering work on the selection of fcc or bcc phases in block copolymer micelles was that of McConnell et al.[21,22] They employed SI diblock copolymers of various *f* and degrees of polymerization (*N*) in the isoprene-selective solvent decane, at room temperature. The micellar ordering structure was determined by the intermicellar interaction potential. The key variable was the ratio of the coronal layer thickness (*L*) to the core radius (R_c). For smaller L/R_c the micelles have relatively thin crew-cut coronal layers.[23] The repulsive interactions between these crew-cut micelles are short-ranged, similar to hard spheres, and thus these systems adopt the close-packed fcc structure. For large L/R_c the micelles are hairy, and their interactions are long-ranged. In this case, the less dense bcc structure is favored. A temperature-induced bcc → fcc transition was observed in aqueous solutions of poly(ethylene oxide)-poly(butylene oxide) (PEO−PBO) diblock copolymers by Hamley and co-workers.[24] At low temperature, PEO is well solvated by water, and the

─────────────

* Author to whom correspondence should be addressed. E-mail: lodge@chem.umn.edu.

† Department of Chemical Engineering and Materials Science.

‡ Department of Chemistry.

bcc structure is formed due to the larger coronal layer of the hydrophilic PEO block. With increasing temperature, PEO becomes less soluble in water and the coronal layer contracts, which results in the fcc structure. Although this phenomenon illustrates the effect of changing solvent quality on the micellar structure, our system is different in the sense that the PS coronal blocks are well-solvated over the entire temperature range. The key factor that affects the structure in this case is the degree of solvent selectivity toward the core PI block, as proposed previously.[20] As the temperature increases, the micelle aggregation number decreases due to core swelling. The resulting micelle is a softer micelle, which allows for the overlap of the coronal chains of interacting micelles. Consequently, the packing arrangement changes from fcc to bcc to accommodate the softer intermicellar potential.

Transformations between bcc and close packed (fcc or hexagonally close packed, hcp) phases have been established in many metal systems such as Fe, Mg, and Zr.[25−33] The hcp ↔ bcc and fcc ↔ bcc transformations follow the "Burgers mechanism" and the "Bain distortion", respectively. Remarkably, the fcc/hcp → bcc transformation in block copolymer solutions is epitaxial, and follows apparently similar pathways as in many metals.

Experimental Section

Materials. Two approximately symmetric poly(styrene-*b*-isoprene) diblock copolymers, designated SI(8−7) and SI(15−15), with block molecular weights of 8.0×10^3 and 7.0×10^3 g/mol, and 1.5×10^4 and 1.5×10^4 g/mol, respectively, were polymerized by living anionic polymerization using standard procedures.[18] The polymers were characterized by size exclusion chromatography (SEC), using both refractive index and multi-angle light scattering detectors (Wyatt Optilab and Dawn), and by ^{1}H NMR. SEC determined the number average block molecular weights, M_{PS} and M_{PI}, and the polydispersities, M_w/M_n of 1.01 and 1.02 for SI(8−7) and SI(15−15), respectively. ^{1}H NMR was used to determine the block composition and to estimate the mole percent of 4,1-addition of the PI block (94 ± 1%). The solvents di-*n*-butyl phthalate (DBP), diethyl phthalate (DEP), dimethyl phthalate (DMP), *n*-tetradecane (C14), and squalane (C30) were purchased from Aldrich and purified by vacuum distillation. The polymer solutions were prepared gravimetrically, with the aid of methylene chloride as a cosolvent. The cosolvent was stripped off under a stream of nitrogen at room temperature until a constant weight was achieved. The polymer volume fraction, ϕ, was calculated assuming additivity of volumes and densities of 1.043, 1.118, 1.160, 0.763, 0.810, 1.047, and 0.913 g/cm^3 for DBP, DEP, DMP, C14, C30, PS, and PI, respectively.

Small-Angle X-ray Scattering (SAXS). The fcc and bcc phases and the transition temperatures were identified by SAXS for unoriented solutions. SAXS measurements were made on the 2 m beam line at the University of Minnesota. CuK$_\alpha$ X-rays ($\lambda = 1.54$ Å) are generated by a Rigaku RU-200BVH rotating anode X-ray generator equipped with an 0.2×2 mm microfocus cathode and collimated with Franks mirror optics. 2D SAXS patterns are detected by a 1024×1024 pixel (each pixel = 100 μm^2) Siemens area detector (HI−STAR Siemens Analytical X-ray Instruments) at the end of an evacuated flight tube. The sample to detector distance was fixed at 2.43 m for most experiments. The collected data were corrected to account for the spatial distortion of the detector surface. The solutions were sealed within 1.5 or 2.0 mm quartz capillaries with a high-temperature silicone based sealant. The measurements were
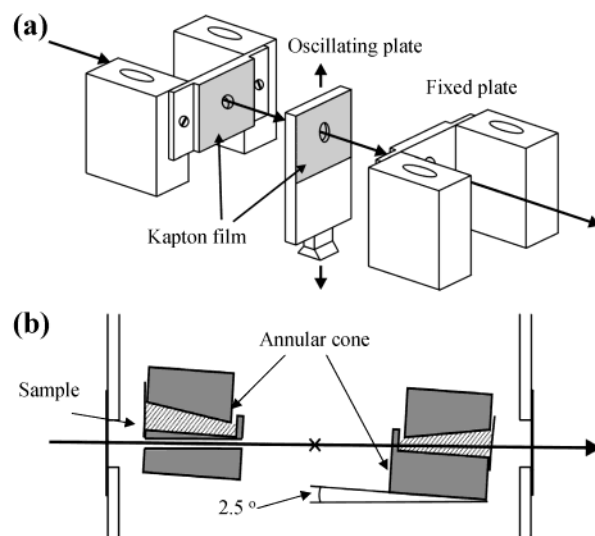
Figure 1. Schematic representation of (a) the shear sandwich configuration in the DMTA and (b) the annular cone and plate shear cell. The cone angle is exaggerated in this image (the actual angle is 5°).

performed by first annealing each sample at a set temperature for at least 600 s, followed by a 300−600 s exposure. The temperature was then changed in small increments and the procedure repeated. The 2-D SAXS images were azimuthally averaged to produce one-dimensional profiles of intensity, *I*, versus wavevector, *q*.

Small-Angle X-ray Scattering (SAXS) in Shear Cells. To study the epitaxial relationship between the fcc and bcc phases, two in situ shear cells were employed, and thus the solutions could be examined along two orthogonal directions (shear gradient and vorticity axes). For the shear gradient direction, a DMTA rheometer (Rheometric Scientific) was installed on the University of Minnesota 6 m SAXS line.[34] The shear plates (12.5 mm × 12.5 mm) were modified with apertures (3 mm in diameter) at the center and covered by Kapton films with a thickness of 50 μm. The temperature control housing also had appropriate entrance and exit holes for the beam. The X-ray beam was allowed to pass through this parallel plate shear sandwich along the gradient direction, as illustrated in Figure 1a. The maximum displacement of the moving plate is 0.5 mm, and the desired strain (γ) range can be varied by controlling the gap size. The samples were sheared in the fcc phase by applying $\gamma = 100\%$ and $\omega = 1$ rad/s for approximately 1 h, and then heated to the bcc phase without shear to observe the epitaxial evolution of the bcc phase.

Additional SAXS measurements were performed using beam line 5ID-D, in the DuPont-Northwestern-Dow (DND-CAT) station at the Advanced Photon Source, Argonne National Laboratory. A 17 keV radiation ($\lambda = 0.73$ Å) was selected from an undulator beam using a double-crystal monochromator then collimated using two sets of slits with a square cross section of 0.2×0.2 mm^2. A sample to detector distance of 6.8 m was used to access the necessary *q* range. 2-D SAXS images were collected using a CCD detector (MAR). A novel cone and plate shear cell[35] was installed in this beam line to access the vorticity direction, as previously described.[36] The central portion of a traditional cone and plate geometry was removed to create annular fixtures with inner and outer radii of 1.5 and 2.5 cm, respectively. A hole was drilled through the fixed lower annular plate, so that the incident X-ray beam passes through the center of the device, then through the sample on the opposite side of the shear cell. The cone angle is 5°, so the shear cell was tilted

Close-Packed and BCC Lattices

J. Phys. Chem. B, Vol. 107, No. 44, 2003 **12073**

to an angle of 2.5° in order for the beam to pass through the cell horizontally, as illustrated in Figure 1b.

Small-Angle Neutron Scattering under Shear. Neutron scattering experiments were conducted at NIST, Gaithersburg, MD, using the NIST/Exxon/University of Minnesota 30 m SANS instrument (NG7). Neutrons with wavelength $\lambda = 6$ Å and $\Delta\lambda/\lambda = 0.11$ were incident on the sample, which was mounted in a large amplitude reciprocating shear machine.[37] The shear plates are made from aluminum to allow passage of the neutrons along the gradient direction. The strategy for the experiments was the same as that in SAXS, and thus the SAXS and SANS experiments should provide essentially equivalent results.

Results and Discussion

We first describe the factors that influence the selection of fcc or bcc phases in these block copolymer solutions. A thermotropic fcc → bcc transition is consistently observed for approximately symmetric polymers in both PS and PI selective solvents, over an appropriate concentration range. In situ SAXS measurements taken along the gradient and vorticity directions provide a clear picture of the transformation epitaxy. In fact, shearing induces a mixture of hcp and fcc phases, and thus mechanisms for both the fcc → bcc and hcp → bcc transformations are proposed. The SAXS patterns are indexed, and the orientation relationships between the parent fcc/hcp mixture and the newly formed bcc phases are discussed in detail.

General Features. As part of an ongoing effort, the phase behavior of six SI diblock copolymers, SI(11−32), SI(11−21), SI(15−13), SI(8−7), SI(22−12), and SI(38−14), in several PS-selective solvents has been explored.[16−19] For each polymer, phase diagrams were constructed as a function of the polymer volume fraction and temperature. Figure 2 illustrates the corresponding phase diagrams for SI(8−7)[18] and SI(15−15) (this work) in DMP. The filled (open) circles represent measured order−disorder (order−order) transitions, and the smooth curves represent estimates of the phase boundaries. These boundaries should in principle be marked by regions of two phase coexistence, but as is generally the case in experiment[16,18,19] and anticipated by theory,[38] these intervals are too narrow to be resolved. As more solvent is added, the effective volume fraction of the polymer is changed due to the preferential swelling of the PS block, and the lyotropic phase transition sequence L → G → C → S → micelle solution is observed. Due to the temperature dependence of the solvent selectivity, a variety of thermotropic order−order transitions occur at particular concentrations. Most importantly for this study, over the approximate range $\phi \approx 0.20-0.40$, the solutions show cubic micellar lattices, with an fcc to bcc transition upon heating. In contrast, solutions for more asymmetric polymers exhibit only fcc or bcc phases, depending on the block composition, f. For small f_{PS} (i.e., for SI(11−32) and SI(11−21)), the micelles have short corona chains. These crew-cut micelles have a relatively short-ranged, steeply repulsive interaction and thus adopt the close-packed fcc lattice. For large f_{PS} (i.e., for SI(22−12) and SI(38−14)), the micelles have long corona chains, and these hairy micelles interact via a softer, longer-ranged repulsion, which favors the less-dense bcc lattice. These observations are qualitatively (but not quantitatively) consistent with the criteria proposed by McConnell et al.[21,22]

For the intermediate regime of symmetric or nearly symmetric copolymers such as SI(8−7) and SI(15−15) ($f_{PS} = 0.49$ and 0.47, respectively), there are thermotropic fcc to bcc transitions. The bcc window near the ODT can be as small as $\Delta T \approx 10$ °C.
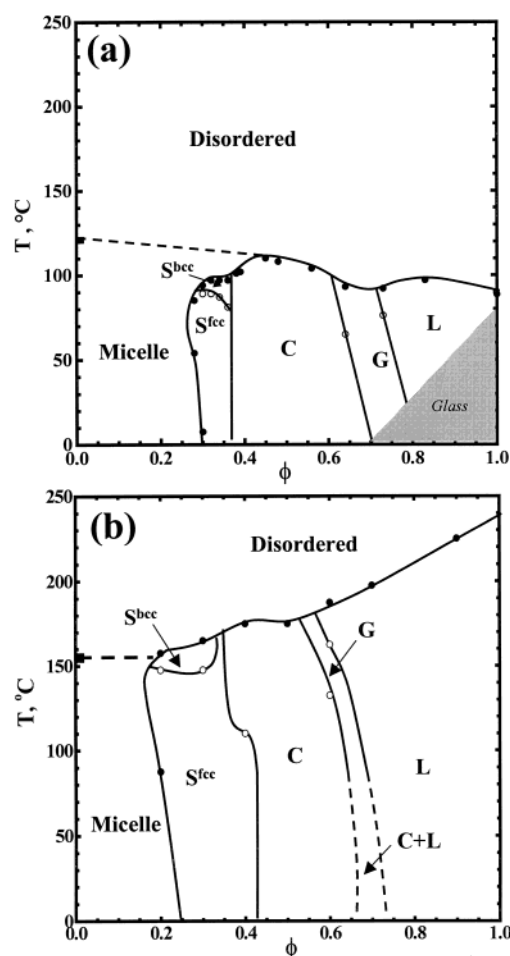

Figure 2. Phase diagrams for (a) SI(8−7) in DMP and (b) SI(15−15) in DMP as functions of temperature, T, and polymer volume fraction, ϕ.

This bcc window, intervening between fcc and disordered liquid, is interesting in that it is reminiscent of many atomic systems.[26−30,39−41] It appears to be an example of the Alexander-McTague conjecture that a bcc phase is generally preferred near the melting line for weakly first-order transitions, for entropic reasons.[41] Ziherl and Kamien have proposed a more explicit argument for copolymer micelles, such that a bcc lattice is favored over a close packed lattice when the micelles have relatively long corona chains. This is because the entropic penalty for corona overlap is lower in bcc, due to the smaller area of the corresponding Wigner-Seitz cell.[42,43] It should also be pointed out that these authors have recently demonstrated that a different cubic packing of micelles, termed A15, could be slightly preferred over either fcc or bcc under some conditions.[42,43] They suggest that A15 structure could be found in micelles with sufficiently long coronas. The experimental signature of A15 would be a series of reflections at $1:\sqrt{2}:\sqrt{2.5}:\sqrt{3}...$; we have not seen a clear indication of this structure to date.

The mechanism for the fcc → bcc transition in this work is determined by SAXS. The transition cannot be observed by static birefringence, because both fcc and bcc phases are optically isotropic. Also, in contrast to most order-order transitions, the dynamic moduli do not display a significant change for this transition, although a small bump is sometimes observed in $G''(T)$ upon heating as the lattice rearranges. Figure 3 displays representative SAXS profiles for fcc, bcc, and
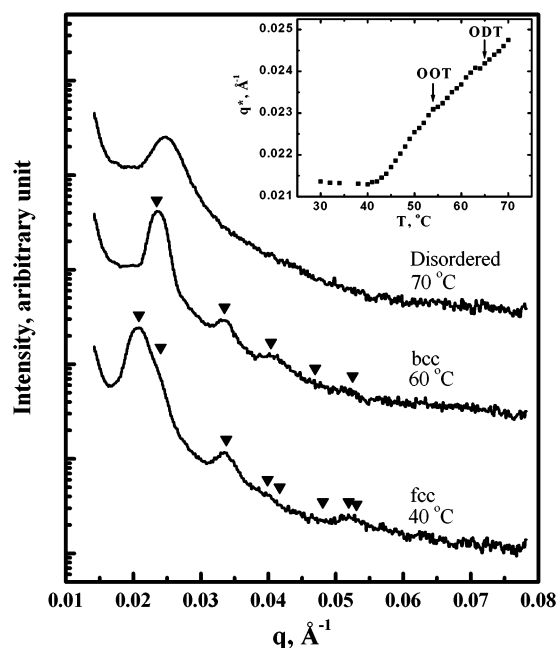
Figure 3. Representative SAXS profiles as a function of temperature for SI(15−15) in DBP/DEP $\phi = 0.20$. The inset shows the temperature dependence of the principal peak position.

TABLE 1: Solution Samples Studied

sample	ϕ	solvent	OOT (°C)	ODT (°C)
SI(8−7)	0.30	DEP	35	50
SI(8−7)	0.35	DEP	35	50
SI(15−15)	0.20	DBP/DEP	55	65
SI(15−15)	0.13	C14	55	80
SI(15−15)	0.20	C30	145	165

disordered phases. The fcc at 40 °C and bcc at 60 °C are identified by the peaks at relative positions $\sqrt{3}:\sqrt{4}:\sqrt{8}:\sqrt{11}:\sqrt{12}:\sqrt{16}:\sqrt{19}:\sqrt{20}$ and $1:\sqrt{2}:\sqrt{3}:\sqrt{4}:\sqrt{5}$, respectively. A bcc phase can be distinguished from a simple cubic (SC) by the presence of the $\sqrt{7}$ $q*$ reflection. The SAXS pattern for bcc in Figure 3 displays only 2 clear higher order peaks due to the weak segregation near the ODT. However, the $\sqrt{7}$ $q*$ reflection was observed in other solutions that show the same fcc → bcc transition. Also, in block copolymer systems, the bcc phase is prevalent, whereas SC is not, and hence we conclude this lattice to be bcc. In addition, the principal spacing of the cubic lattices, $2\pi/q*$, decreases smoothly across the transition (inset to Figure 3), suggesting that the number of micelles does not change abruptly during the transition. The decrease in the domain spacing implies a decrease in the micellar size and/or an increase in the number density of micelles, and thus the mean aggregation number of micelles decreases with increasing temperature. A full description of the micelle structure with varying temperature will be discussed in a subsequent report.

The solution samples examined in this study are listed in Table 1. To investigate the epitaxial relationship between fcc and bcc phases, the following strategy was adopted. The solution was sheared in the fcc phase and then annealed without shear. The sample was then heated to within the bcc phase in the absence of shear, to observe how the bcc phase grows epitaxially. We have examined these solutions by SAXS in two in situ shear cells to investigate the scattering along two orthogonal axes: the shear gradient (∇) and the vorticity (**e**) directions.

Scattering Patterns Along the Gradient Axis. The solution samples were sheared in the DMTA parallel plate rheometer,
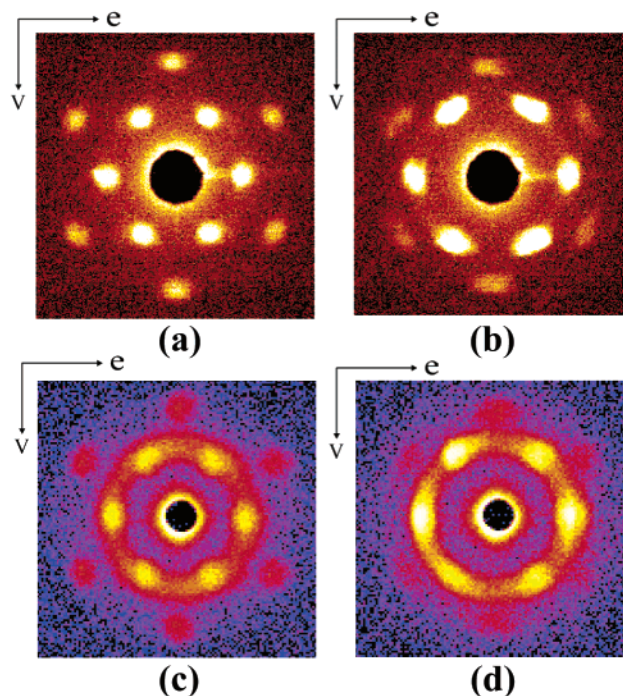
Figure 4. SAXS ((a) and (b)) and SANS ((c) and (d)) patterns in the gradient direction for the fcc ((a) and (c)) and bcc structures ((b) and (d)) of SI(15−15) in DEP/DBP $\phi = 0.20$. The sample is sheared at 45 °C (fcc) then heated to 60 °C (bcc) without shear.
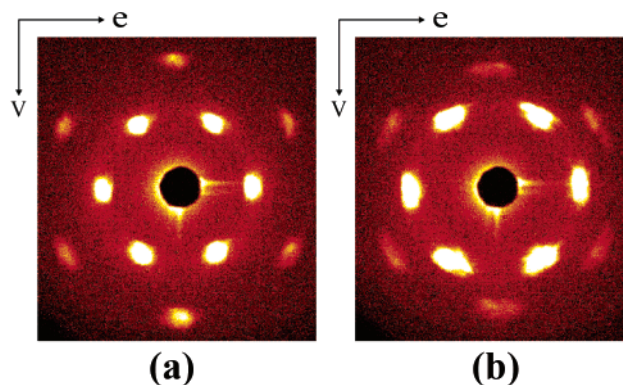
Figure 5. SAXS patterns for SI(8−7) in DEP $\phi = 0.30$ in the gradient direction (a) after shearing in the parallel plate at 30 °C (fcc/hcp) and (b) after heating to 40 °C (bcc) without shear.

and a well-developed SAXS pattern was obtained within an hour. As shown in Figure 4a for SI(15−15) in a DEP/DBP mixture, $\phi = 0.20$, and in Figure 5a for SI(8−7) in DEP with $\phi = 0.30$, there are six first-order spots and six second-order spots at larger q, with hexagonal symmetry. This scattering pattern is characteristic of shear-oriented close-packed colloidal or micellar systems and has been well-documented;[22,24,44−58] the densest {111} planes are oriented in the velocity (**v**)−vorticity (**e**) plane, with the close-packed direction along **v**. After turning off the shear, the solution was then heated slowly to a temperature within the bcc phase. After 10 min, the transformation was essentially complete, and only the bcc phase was observed (Figures 4b and 5b). The main features are that (i) all 12 spots clearly remain at the same angular positions; (ii) the peaks in the bcc phase are significantly smeared azimuthally; (iii) the $q/q*$ ratio changes, such that the six first-order spots have moved to larger q, and the six outer spots have moved to smaller q, with $q/q* = \sqrt{2}$, characteristic of the bcc phase; and (iv) the relative intensity of the first order to the second-order

Close-Packed and BCC Lattices

J. Phys. Chem. B, Vol. 107, No. 44, 2003 **12075**

peaks is greater in bcc. The same type of experiment was performed using SANS on the same SI(15−15) solution as that in Figure 4, parts a and b. After shearing at a frequency of 0.03 Hz and a strain amplitude of 400%, equivalent results to SAXS were obtained (see Figure 4, parts c and d). Due to the lower resolution of SANS compared to SAXS, the SAXS patterns are emphasized in the further analysis. The fact that spots are clearly observed both prior to and after the transition, coupled with the continuous change of the domain spacing across the transition, establishes that there is an epitaxial relationship between the fcc and bcc structures.

For the "fcc" scattering patterns in Figures 4a, 4c, and 5a, it should be noted that the inner six spots are actually due to the hcp stacking of the {111} plane. A perfect fcc crystal with {111} planes normal to the shear gradient direction would give no first-order reflections, as none of the {111} planes in the fcc unit cell can be oriented parallel to the beam direction.[45,46,48] When shearing the fcc micellar solution, the favored slip planes are the densest {111} planes, as is well documented in the literature.[22,24,44−58] Among the possibilities for stacking the {111} planes are an ABCABC stacking, which produces the fcc structure, and an ABAB stacking, which corresponds to the hcp structure. Thus, the sheared "fcc" solution is actually a combination of fcc and hcp stacking. We assume that the stacking sequence is effectively random along the gradient direction throughout the macroscopic sample, although distinct "grains" containing multiple layers of perfect registry are certainly possible. These issues have been discussed elsewhere.[22,58] In the absence of the symmetry-breaking flow field, the essentially degenerate fcc and hcp states may be simply considered to be close packed spheres.

The coexistence of the hcp and fcc structures after shear is also confirmed by the following feature. Figure 6 displays a scattering pattern obtained during the early stages of shearing the same solution as in Figure 4. The six bright hcp spots are superposed on a powder pattern in the first peak position. After integrating over appropriate sectors as illustrated in Figure 6a, the sector labeled **1** gives a q ratio of $\sqrt{8}/\sqrt{3}$ (see Figure 6b), characteristic of fcc. This suggests that the powder pattern arises from the {111} reflection of fcc. However, after measuring the q position of the first-order bright spots (sector **2**), the q ratio with the second-order spot appears at $\sqrt{3}$ (see Figure 6c), which supports the hypothesis that the first-order spots arise from hcp. As expected from this feature, the q/q^* ratio in Figures 4a and 5a is $\sqrt{3}$, consistent with the hcp structure, rather than the $\sqrt{8}/\sqrt{3}$ which is expected for fcc. Therefore, we assign the first-order peaks in Figures 4a and 5a to the {10$\bar{1}$0} planes in the hcp structure, but the second-order peaks come from both the hcp and fcc structures (i.e., {220} planes in fcc and {11$\bar{2}$0} planes in hcp). This indexing is shown in Figure 7a.

Figure 7b shows the indexed pattern for the bcc phase after the transformation. The azimuthally smeared peaks (both 110 and 200 reflections) are indexed as groups of three closely spaced spots, indicating a total of nine different orientations of the bcc unit cells, as will be discussed later. Also, as noted previously, the intensity of the 110 reflections in the bcc phase has increased relative to the hcp precursors, as quantified in Figure 8. From the azimuthal integration of the first-order peaks, one can see the increase in the intensity of the bcc peaks (albeit not uniformly at the various angular positions) as well as the broadening. Similarly, the second-order peaks decrease in integrated intensity after the transition (data not shown).

Because we have used symmetric diblocks, the same phase behavior should be expected when comparable PI selective
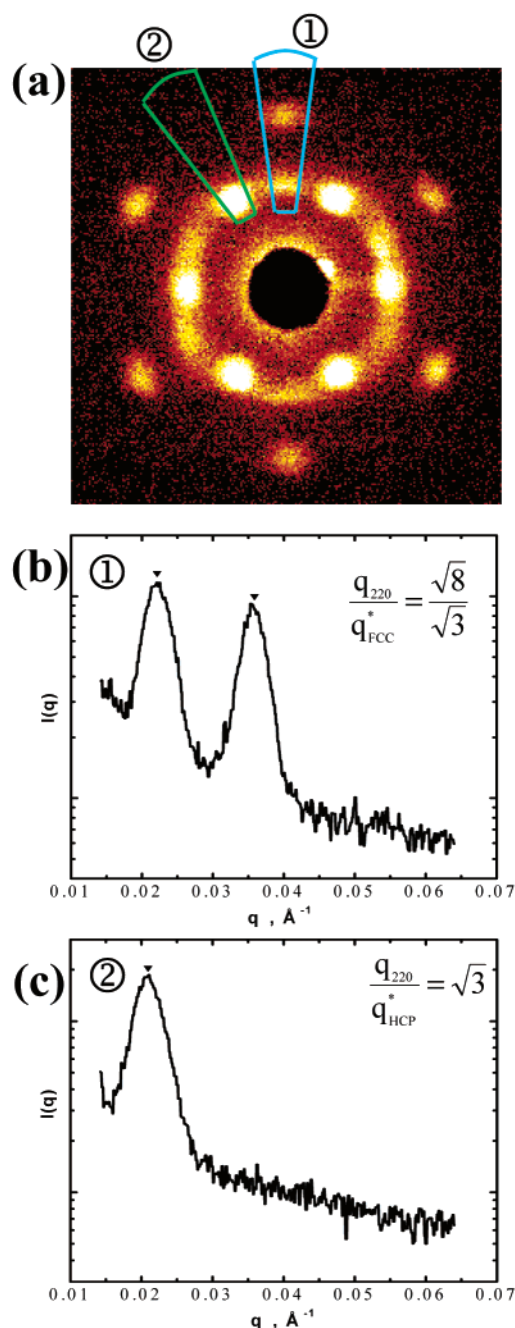
Figure 6. (a) SAXS pattern for the early stages of the sheared fcc/hcp mixture of SI(15−15) in DEP/DBP $\phi = 0.20$ in the gradient direction. (b) and (c) represent the SAXS profiles after integrating over sectors **1** and **2**, respectively.

solvents are employed. Indeed, we have found the same fcc → bcc transitions in C14 and C30 solutions of SI(15−15), as shown in Figure 9. In this case, higher order peaks such as the coincident 440 reflections in fcc and 20$\bar{2}$0 reflections in hcp were observed (presumably due to the greater X-ray contrast in C14 and C30 solutions). In the C30 solution, the SAXS pattern for the bcc phase is not shown, because the transition temperature is so high (ca. 150 °C) that the solvent could evaporate during the measurement. This symmetry of response between PS-selective and PI-selective solvents is gratifying, particularly because the fcc → bcc transition was not observed in previous studies in PI-selective solvents. For example, McConnell et al. investigated the selection of fcc or bcc phases by employing several SI diblocks in the isoprene selective
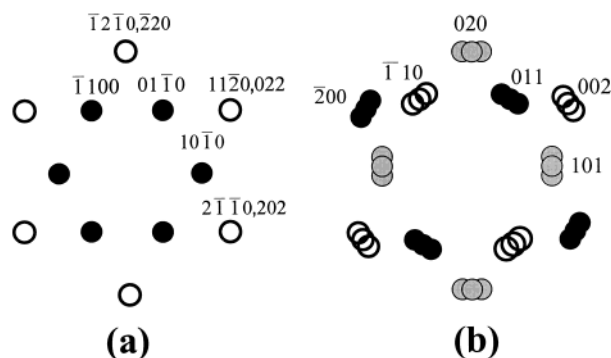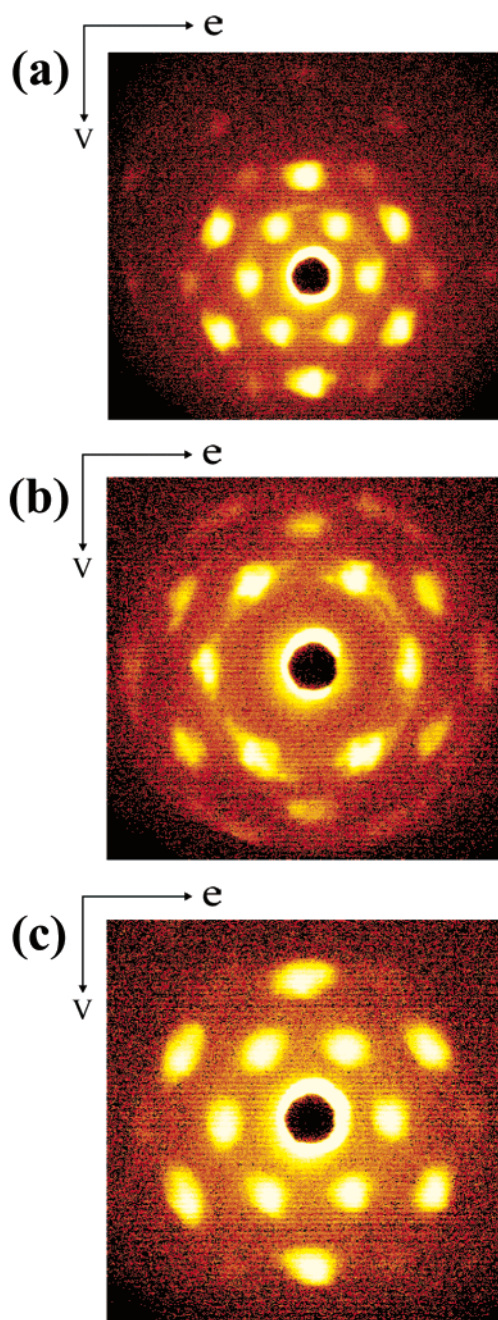
Figure 7. Indexing of SAXS patterns for (a) fcc/hcp and (b) bcc structures in the gradient direction.
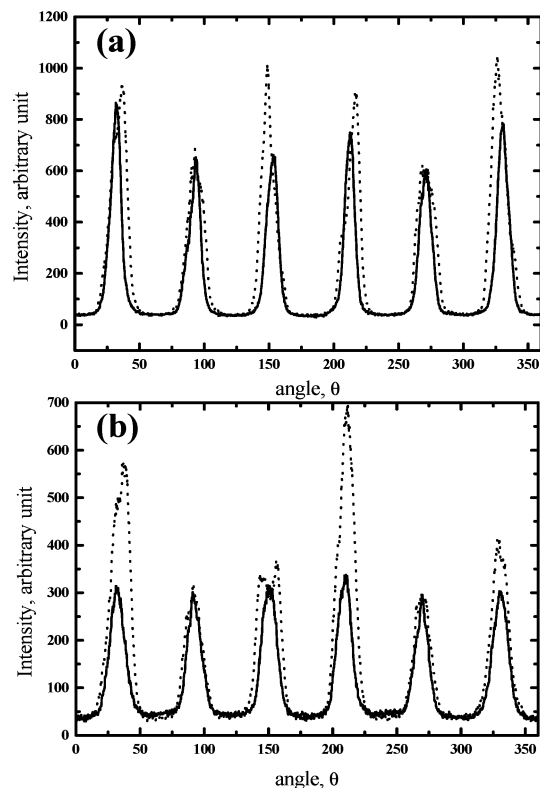
Figure 8. Azimuthal integrations of SAXS intensities for the first-order peaks (a) in Figure 4, parts a and b, and (b) in Figure 5, parts a and b. The solid lines correspond to the $10\bar{1}0$ reflections of hcp and the dotted lines to the 110 reflection of bcc.


Figure 9. SAXS patterns in the gradient direction for the (a) fcc/hcp and (b) bcc structures of SI(15−15) in C14 $\phi = 0.13$ and (c) fcc/hcp structure of SI(15−15) in C30 $\phi = 0.20$.

solvent decane.[22] All the measurements were performed at a fixed temperature, so no thermotropic fcc → bcc transition was observed. Lai et al. employed SI diblocks in the isoprene selective solvents tetradecane, squalane, and tributylamine, and investigated the phase behavior over a wide range of concentration and temperature.[59] The overall features are certainly consistent with our previous results, even though there are differences as pointed out previously.[18] However, they did not observe fcc phases, or fcc → bcc transitions in any solutions, most likely because the emphasis was on the higher concentration regime.

Scattering Patterns Along the Vorticity Axis. One sample, SI(8−7) in DEP with $\phi = 0.35$, was examined in the modified cone and plate shear cell at the Advanced Photon Source. The shear and heating procedures were the same as those in the previous experiments. Figure 10, parts a and b display the SAXS patterns of fcc/hcp and bcc, respectively, viewed along the vorticity direction. Comparing to Figures 4 and 5, there are more

higher order reflections in both fcc/hcp and bcc patterns, and the peaks are sharper. This reflects the higher flux and superior collimation available with the synchrotron. Figure 10a corresponds to a superposition of fcc and hcp SAXS patterns viewed in the [112] and [10$\bar{1}$0] beam directions, respectively, with $\{111\}_{fcc}$ ($\{0002\}_{hcp}$) planes oriented along the shear direction, as indexed in Figure 11. Note that the scattering patterns of fcc and hcp in the vorticity direction should be identical. Because the SAXS patterns in the gradient direction show a mixture of fcc and hcp phases (Figures 4a and 5a), Figure 10a is consistent with the same mixture. There are four additional spots on the inner ring, positioned at ca. $\pm 50°$ from the main 111 reflections. These can be regarded as a small population of $\{111\}$ planes oriented at $\pm 50°$ relative to the shear plane. The intensity of these reflections is less than 1% of those of the main 111 reflections, so their population is relatively small. We tentatively
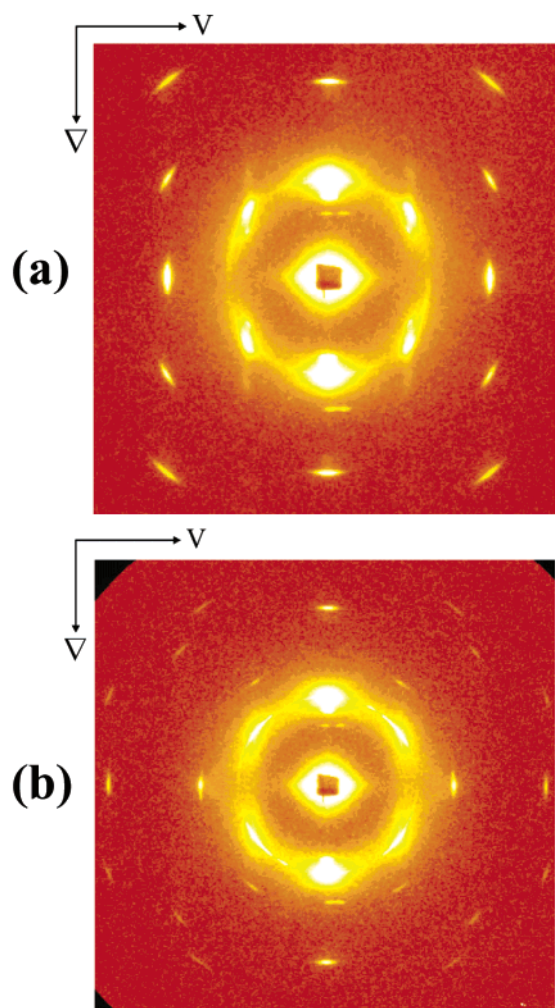
Figure 10. SAXS patterns for SI(8−7) in DEP $\phi = 0.35$ in the vorticity beam direction (a) after shearing in the cone and plate at 30 °C (fcc/hcp), then (b) after heating to 40 °C (bcc) without shear.
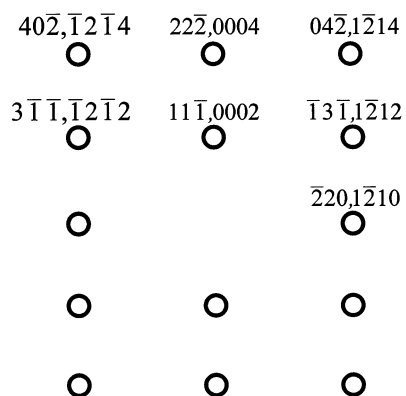
Figure 11. Indexing of SAXS pattern for the fcc/hcp mixture in the vorticity direction.

attribute these (at least in part) to misaligned {111} planes near the inner and outer surfaces of the flow cell, where the flow profile is inevitably inhomogeneous.

After heating to 40 °C without shear, the resulting bcc scattering pattern is shown in Figure 10b. There are also a number of higher order peaks, and as will be demonstrated subsequently, they can be assigned to a superposition of the bcc patterns viewed along the ⟨110⟩ and ⟨112⟩ directions.[60] This indicates that the bcc unit cells have at least two different orientations after transformation from the fcc/hcp mixed crystal.
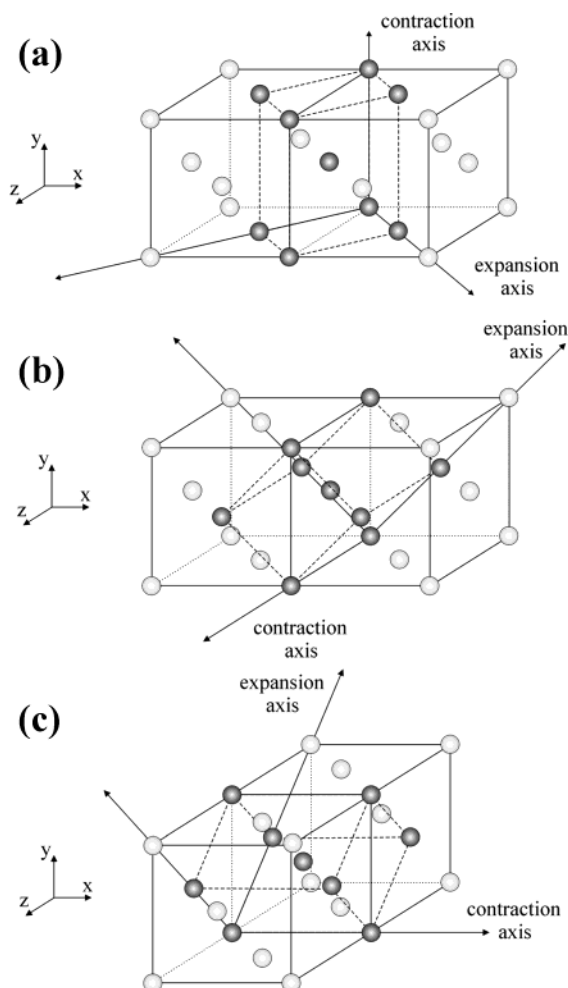
Figure 12. Illustration of the Bain distortion. Distorted bcc unit cell imbedded (dark spheres) in two fcc unit cells. A 3-fold degeneracy in the Bain distortion leads to three different sets of the Bain distortion axes for the transformation as shown in (a), (b), and (c).

Furthermore, the bright spots shown in the vertical axis correspond to the 110 and 220 reflections, which come from stacking of the {110} planes. This feature suggests that the densest planes ($\{111\}_{fcc}$ and $\{110\}_{bcc}$) remain parallel during the transformation. The "misaligned" fcc planes evident in Figure 10a also have their counterparts in Figure 10b, with even some corresponding higher order peaks now evident.

Epitaxial Relationships. We now turn to the epitaxial relationships between the parent fcc/hcp and the daughter bcc phases. Because shearing the fcc solution produces a mixture of hcp and fcc phases, and then this mixture transforms to the bcc phase, there are actually two epitaxial transformations superimposed: hcp → bcc and fcc → bcc. Both transformations have been observed in many atomic systems.[25−33]

The fcc → bcc transformation is commonly described via the well-known Bain distortion,[25−28,31] illustrated schematically in Figure 12. A distorted bcc unit cell imbedded in two fcc unit cells transforms to a bcc unit cell by compressing along one ⟨100⟩ direction and expanding along two ⟨110⟩ directions of the fcc unit cell. There is a 3-fold degeneracy with respect to the contraction axis, as it can be any of three orthogonal axes. Hence, the Bain distortion can occur in three directions: contraction along the [010], [001], or [100] direction, with corresponding expansion along [101] and [$\bar{1}$01], [110] and [$\bar{1}$10], or [011] and [01$\bar{1}$] directions, respectively (shown in Figure 12, parts a, b, and c, respectively). As a result of the Bain

distortion, the bcc unit cells will have three different orientations with {200} planes along the shear gradient direction, and the six second order spots in Figures 4b and 5b could be so assigned. However, this "pure" Bain distortion has some difficulties with respect to the experiments. First, the smearing of the bcc peaks cannot easily be explained. Second, the intensity of the first order peak in Figures 4b and 5b increased during the transformation, as shown in Figure 9. The first order spots in Figures 4a and 5a are purely from hcp stacking, and no increase in the intensity would be expected if only the hcp → bcc transformation is involved in the first-order peaks. It is possible that the fcc → bcc transformation also contributes to the 110 reflections, but the pure Bain distortion would not give such 110 reflections, because no {110} planes are aligned along the gradient direction. Third, two superimposed SAXS patterns for the bcc phase are observed in the vorticity direction, which is also not consistent with the "pure" Bain distortion. The "pure" Bain distortion would not allow any reflections, because none of the planes in bcc unit cells would be oriented parallel to the vorticity beam direction. Finally, the crucial feature from the fcc/hcp and bcc patterns in the vorticity direction is that the densest planes in fcc, hcp, and bcc remain parallel during the transformation: $\{111\}_{fcc} \| \{110\}_{bcc}$ and $\{10\bar{1}0\}_{hcp} \| \{110\}_{bcc}$. This implies that certain orientation relationships (ORs) exist between the parent fcc/hcp and the daughter bcc phases. As a result, a modified Bain distortion, consisting of infinitesimal axis distortion and rotation in addition to the "pure" Bain distortion, is needed to satisfy the particular OR.

The OR between two different crystals is common in many metal systems.[25,61−67] Studies have focused on how a precipitate is oriented relative to its surrounding matrix, a fiber to the adjacent matrix, a thin film to the substrate, or two grains oriented at either side of a grain boundary. The best-known ORs are between cubic and close packed structures (fcc, hcp, bcc, etc.). For example, if an fcc precipitate (α) forms inside an fcc matrix (β), then one may find ORs such as $[100]_\beta \| [100]_\alpha$ and $(010)_\beta \| (010)_\alpha$.

Several studies have focused on the deposition of fcc metals on bcc substrates ($\{110\}_{bcc}$ surface).[61−64,67] In this case, there are two special kinds of epitaxial ORs in which the closest-packed planes in the fcc and bcc phases are parallel. One is the Kurdjumov-Sachs (K−S) OR: $(111)_{fcc}\|(110)_{bcc}$ (the closest-packed planes), $[\bar{1}10]_{fcc}\|[\bar{1}11]_{bcc}$ (the closest-packed directions), and $[11\bar{2}]_{fcc}\|[1\bar{1}2]_{fcc}$. The other is the Nishiyama-Wassermann (N−W) OR: $(111)_{fcc}\|(110)_{bcc}$ (the closest-packed planes), $[\bar{1}01]_{fcc}\|[001]bcc$, and $[12\bar{1}]_{fcc}\|[\bar{1}10]_{bcc}$. The K−S and N−W ORs are frequently encountered relationships for bcc-fcc systems and differ from each other by a small relative rotation of $5.26°$.[65−67] The main difference is that both the closest planes and directions remain parallel in the K−S OR, whereas only the closest planes remain parallel in the N−W OR. It has also been found that there exist ORs between the parent and daughter phases in martensitic transformations.[25−27,31] These relations suggest that it is possible to describe the process of transformation by homogeneous deformation of the initial lattice by contraction and/or dilation parallel to particular planes and/or directions.

Figure 13 shows the possible orientations of the bcc unit cell after the modified Bain distortion. The light spheres lie in {111} planes of the fcc structure before transformation, and the dark spheres represent {110} planes of the bcc unit cell after transformation. Comparing Figures 12 and 13, three distinct orientations of the bcc unit cells are produced for each contraction axis. Two have closest-packed directions that are
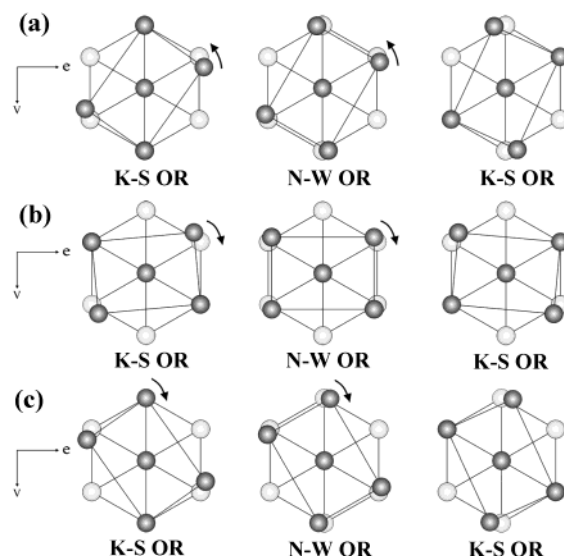
Figure 13. Superposition of close-packed {111} fcc (light spheres) and {110} bcc planes (dark spheres). Compressing along one direction, two K−S and one N−W ORs are obtained. In total, nine orientations of the bcc unit cell are created. The orientations of the bcc unit cells in (a), (b), and (c) are the results of the Bain distortion in Figure 12, parts a, b, and c, respectively.

coincident between fcc and bcc, as well as closest-packed planes (i.e., the K−S OR). The third is N−W OR that is obtained from either K−S ORs by a $5.26°$ in-plane rotation. As a result, this 3-fold degeneracy for each contraction axis gives rise to nine orientations of the bcc unit cell (six K−S and three N−W ORs). Numerical calculation of the interfacial energy of the fcc and bcc interface reveals that the preference for K−S and N−W ORs depends on the diameter ratio between fcc and bcc spheres.[66] However, the calculation cannot predict the preferred orientation for similar diameter ratios ($0.96 < d_{bcc}/d_{fcc} < 1.02$), because the interfacial energy is negligibly different between both ORs. Hence both K−S and N−W ORs can be considered for the fcc → bcc transformation, as the domain spacing is continuous during the transformation ($d_{bcc}/d_{fcc} \approx 1$). Table 2 summarizes the possible ORs between the parent fcc and the nine bcc unit cells.

In the gradient direction, all nine bcc unit cells give rise to the scattering in the $\langle 110 \rangle$ beam directions, so there are 18 110 and 18 200 reflections in total as indexed in Figure 7b. Each group of three spots exhibits two K−S and one N−W ORs from the Bain distortion along one contraction axis, which nicely accounts for the azimuthal smearing in Figures 4b and 5b. However, only three bcc unit cells hold the ORs with the vorticity beam direction (the [112] direction in the fcc unit cell). They are bcc 1, 5, and 7 in Table 2, and the scattering pattern can be indexed as a superposition of the reflection patterns in three beam directions (Figure 14c); the $[2\bar{1}1]$ and $[1\bar{1}2]$ directions (Figure 14a, two of the six K−S ORs) and the [101] direction (Figure 14c, one of the three N−W ORs). For the other bcc unit cells, the ORs do not provide an axis parallel to the vorticity beam direction, and therefore, reflections occur only for stacking of {110} planes. This is consistent with the fact that the intensity of the main 110 reflections does not change between Figures 10a and b, whereas those of the other higher order peaks decrease significantly. Also, it should be noted that the 121 reflections are diminished due to the form factor minimum. (This is confirmed with the unoriented sample prepared by heating to the disordered phase, then cooling back to 40 °C. In this case, the 121 reflection was still absent (data not shown).) Furthermore, the intensity of the higher order peaks

Close-Packed and BCC Lattices

J. Phys. Chem. B, Vol. 107, No. 44, 2003 **12079**

TABLE 2: Epitaxial Orientation Relationships[a]

| name	orientation relationship	note	principal axes transformation
bcc 1	[11$\bar{1}$]$_{fcc}$ || [01$\bar{1}$]$_{bcc}$, [1$\bar{1}$0]$_{fcc}$ || [1$\bar{1}\bar{1}$]$_{bcc}$, [1$\bar{1}$2]$_{fcc}$ || [211]$_{bcc}$	K–S OR	[010]$_{fcc}$ → [010]$_{bcc}$ (contraction axis),
bcc 2	[11$\bar{1}$]$_{fcc}$ || [01$\bar{1}$]$_{bcc}$, [101]$_{fcc}$ || [100]$_{bcc}$, [1$\bar{2}$1$\bar{}$]$_{fcc}$ || [01$\bar{1}$]$_{bcc}$	N–W OR	[$\bar{1}$01]$_{fcc}$ → [100]$_{bcc}$,
bcc 3	[11$\bar{1}$]$_{fcc}$ || [01$\bar{1}$]$_{bcc}$, [011]$_{fcc}$ || [111]$_{bcc}$, [2$\bar{1}$1]$_{fcc}$ || [2$\bar{1}\bar{1}$]$_{bcc}$	K–S OR	[$\bar{1}$01]$_{fcc}$ → [001]$_{bcc}$
bcc 4	[11$\bar{1}$]$_{fcc}$ || [10$\bar{1}$]$_{bcc}$, [101]$_{fcc}$ || [1$\bar{1}$1]$_{bcc}$, [$\bar{1}$21$\bar{}$]$_{fcc}$ || [121]$_{bcc}$	K–S OR	[001]$_{fcc}$ → [001]$_{bcc}$ (contraction axis),
bcc 5	[11$\bar{1}$]$_{fcc}$ || [10$\bar{1}$]$_{bcc}$, [1$\bar{1}$0]$_{fcc}$ || [0$\bar{1}$0]$_{bcc}$, [11$\bar{2}$]$_{fcc}$ || [101]$_{bcc}$	N–W OR	[1$\bar{1}$0]$_{fcc}$ → [100]$_{bcc}$,
bcc 6	[11$\bar{1}$]$_{fcc}$ || [10$\bar{1}$]$_{bcc}$, [011]$_{fcc}$ || [111]$_{bcc}$, [2$\bar{1}$1]$_{fcc}$ || [1$\bar{2}$1]$_{bcc}$	K–S OR	[1$\bar{1}$0]$_{fcc}$ → [010]$_{bcc}$
bcc 7	[11$\bar{1}$]$_{fcc}$ || [110]$_{bcc}$, [1$\bar{1}$0]$_{fcc}$ || [1$\bar{1}\bar{1}$]$_{bcc}$, [1$\bar{1}$2]$_{fcc}$ || [1$\bar{1}\bar{2}$]$_{bcc}$	K–S OR	[100]$_{fcc}$ → [100]$_{bcc}$ (contraction axis),
bcc 8	[11$\bar{1}$]$_{fcc}$ || [110]$_{bcc}$, [011]$_{fcc}$ || [00$\bar{1}$]$_{bcc}$, [2$\bar{1}$1]$_{fcc}$ || [1$\bar{1}$0]$_{bcc}$	N–W OR	[01$\bar{1}$]$_{fcc}$ → [010]$_{bcc}$,
bcc 9	[111$\bar{}$]$_{fcc}$ || [110]$_{bcc}$, [101]$_{fcc}$ || [1$\bar{1}$1]$_{bcc}$, [1$\bar{2}$1$\bar{}$]$_{fcc}$ || [$\bar{1}$12]$_{bcc}$	K–S OR	[01$\bar{1}$]$_{fcc}$ → [001]$_{bcc}$

[a] ∇ = [11$\bar{1}$], V = [1$\bar{1}$0], **e** = [112].
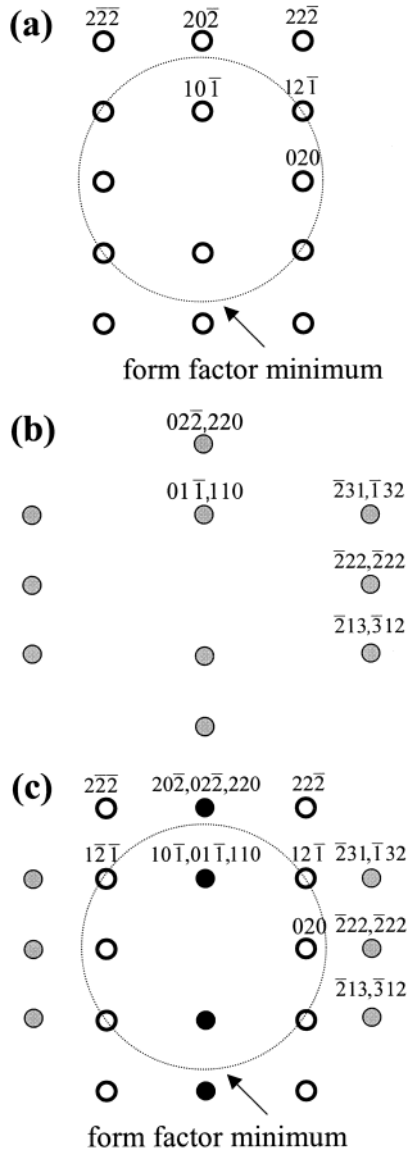
Figure 14. Indexing of SAXS patterns for the bcc structure in the vorticity direction. (a) is the diffraction pattern in the [101] beam direction, and (b) in the [211] and [1$\bar{1}$2] beam directions. (c) is a superimposition of (a) and (b).

in the bcc pattern is much weaker than those in the fcc/hcp pattern. For example, the 200 reflection in bcc is about five times weaker than 220 reflection in fcc, even though {220} planes in fcc transform to {200} planes in bcc. This is consistent with the multiplicity of the orientations in the bcc unit cell.

The hcp → bcc transformation is described in Figure 15. This transformation is known as the Burgers mechanism in the martensitic transformation.[29,30,33] The bcc structure can be
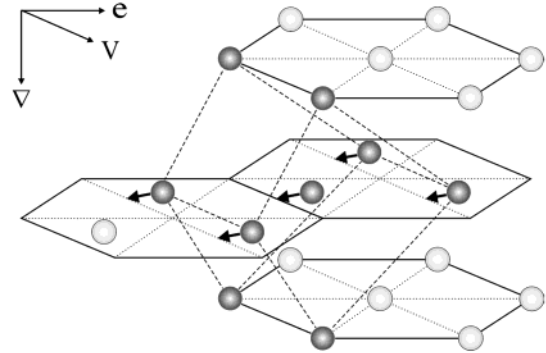
Figure 15. Mechanism of the hcp → bcc transformation. Distorted bcc is imbedded in the hcp structure. Arrows indicate the movement of spheres.

derived from the hcp structure by slippage of alternating {0002} planes along a ⟨$\bar{1}$010⟩ direction, producing the bcc 110 reflection, followed by a slight compression along the {10$\bar{1}$0} planes and expansion along the {1$\bar{2}$10} planes. This produces a bcc crystal with {110} planes stacked along the shear gradient direction. Note that there is also a 3-fold degeneracy in this transformation, just as in the modified Bain distortion. The spheres in alternating {0002} planes can move in any three ⟨$\bar{1}$010⟩ directions: [$\bar{1}$010], [01$\bar{1}$0], and [1$\bar{1}$00]. As with the fcc → bcc transformation, each movement of the spheres in one direction leads to three orientations of the bcc unit cell; two Burgers and one Pitsche-Schrader ORs, which are analogous to the K–S and N–W ORs, respectively.[65] Consequently, the hcp → bcc transformation results in the same nine orientations of the bcc unit cells, as does the fcc → bcc transformation.

As mentioned earlier, the first order spots in Figures 4a and 5a are purely from the hcp stacking, while the second-order spots are both from fcc and hcp. Because both the hcp → bcc and fcc → bcc transformations give rise to the same nine orientations of the bcc unit cell, all the spots in the bcc pattern from Figures 4b and 5b are from both transformations. Therefore, the increased intensity in Figure 8 in the bcc 110 reflections along the gradient direction is a direct consequence of the additional contribution from the fcc → bcc transformation.

One of the main features in the fcc → bcc and hcp → bcc transformations is that the closest-packed planes in fcc and bcc remain parallel during the transformation. It may be more transparent to view the modified Bain distortion as a relative slippage of the closest-packed planes, which is very similar to the Burgers mechanism, as described by Wentzcovitch and Krakauer.[32] In this case, the modified Bain distortion is re-interpreted as follows; compression along the [010] direction is equivalent to the slippage of (11$\bar{1}$) planes in the [$\bar{1}$21] direction, and the internal angle of the (111) layers is deformed from 60° to 70.52°. This description of the fcc → bcc transformation is completely equivalent to that of the hcp →

bcc in that both transformations can be described as the relative slippage of the closest-packed planes, followed by small in-plane deformations. The difference is that the fcc → bcc transformation involves relative motion of A, B and C layers along the same ⟨121⟩ direction, whereas the hcp → bcc transformation involves A and B planes slipping in opposite directions.

Conclusion

SAXS measurements of the hcp → bcc and fcc → bcc transformations in two different orthogonal directions provides a definitive picture of their epitaxial relationships. The main features in these transformations are as follows:

1. Shearing an fcc phase leads to a mixture of hcp and fcc phases due to the random stacking of the densest {111} slip planes. ABC type stacking produces fcc, while AB type stacking produces hcp. Because this mixture transforms to the bcc phase, there are two transformations involved; hcp → bcc and fcc → bcc transformations.

2. The fcc → bcc transformation in this study cannot be simply explained by the "pure" Bain distortion. The modified Bain distortion involves infinitesimal axial distortion and rotation as well as the "pure" Bain distortion, to obey the ORs between the parent fcc and the daughter bcc phases. It is more transparent to describe this transformation in terms of the relative slippage of the close-packed planes ({111} planes), similar to the hcp → bcc transformation (Burgers mechanism). In this case, the slipping directions are same in both transformations. The only difference is that in the fcc → bcc transformation, all the {111} planes slip along the same direction, while in the hcp → bcc transformation, two adjacent planes slip in the opposite direction.

3. In both transformations, there are three degenerate slipping directions. Slipping in one direction generates three orientations of the bcc unit cell by in-plane rotations of 0, ± 5.26°; one corresponds to Nishiyama-Wassermann (or Pitsche-Schrader) OR, and the other two have Kurdjumov-Sachs (or Burgers) ORs. In total, nine orientations of the bcc unit cell are produced, and they are identical for both transformations.

4. In the shear gradient direction, all nine orientations of the bcc unit cell give rise to the scattering. Smearing of the bcc peaks consistent with three orientations of the bcc unit cell is observed in each slipping direction. In the vorticity direction, the scattering patterns arise only from three orientations of the bcc unit cell, except for the layer stacking. They are viewed as a superposition of the scattering patterns in the [10$\bar{1}$] beam direction (one of the three N−W ORs) and the [1$\bar{1}$2] and [211] directions (two of the six K−S ORs).

5. These mechanisms and the resulting ORs between fcc/hcp and bcc are consistent with the analogous martensitic transformations in simple metals. This striking similarity between the block copolymers and the atomic systems suggests an appealing universality of these transitions among the various systems.

References and Notes

(1) Hamley, I. W. *The Physics of Block Copolymers*; Oxford University Press: New York, 1998.

(2) Bates, F. S.; Fredrickson, G. H. *Annu. Rev. Phys. Chem.* **1990**, *41*, 525.

(3) Sakurai, S.; Kawada, H.; Hashimoto, T.; Fetters, L. J. *Macromolecules* **1993**, *26*, 5796.

(4) Koppi, K. A.; Tirrell, M.; Bates, F. S. *J. Rheol.* **1994**, *38*, 999−1027.

(5) Sakurai, S.; Hashimoto, T.; Fetters, L. J. *Macromolecules* **1996**, *29*, 740.

(6) Ryu, C. Y.; Lodge, T. P. *Macromolecules* **1999**, *32*, 7190.

(7) Hajduk, D. A.; Gruner, S. M.; Rangarajan, P.; Register, R. A.; Fetters, L. J.; Honeker, C.; Albalak, R. J.; Thomas, E. L. *Macromolecules* **1994**, *27*, 490.

(8) Hajduk, D. A.; Takenouchi, H.; Hillmyer, M. A.; Bates, F. S.; Vigild, M. E.; Almdal, K. *Macromolecules* **1997**, *30*, 3788.

(9) Hajduk, D. A.; Ho, R.-M.; Hillmyer, M. A.; Bates, F. S.; Almdal, K. *J. Phys. Chem. B* **1998**, *102*, 1356.

(10) Schulz, M. F.; Bates, F. S.; Almdal, K.; Mortensen, K. *Phys. Rev. Lett.* **1994**, *73*, 86−89.

(11) Lodge, T. P.; Pan, C.; Jin, X.; Liu, Z.; Zhao, J.; Maurer, W. W.; Bates, F. S. *J. Polym. Sci., Polym. Phys. Ed.* **1995**, *33*, 2289.

(12) Lodge, T. P.; Xu, X.; Ryu, C. Y.; Hamley, I. W.; Fairclough, J. P. A.; Ryan, A. J.; Pedersen, J. S. **1996**.

(13) Lodge, T. P.; Hamersky, M. W.; Hanley, K. J.; Huang, C.-I. *Macromolecules* **1997**, *30*, 6139.

(14) Hamley, I. W.; Fairclough, J. P. A.; Ryan, A. J.; Ryu, C. Y.; Lodge, T. P.; Gleeson, A. J.; Pedersen, J. S. *Macromolecules* **1998**, *31*, 1188.

(15) Huang, C.-I.; Lodge, T. P. *Macromolecules* **1998**, *31*, 3556.

(16) Hanley, K. J.; Lodge, T. P. *J. Polym. Sci., Polym. Phys. Ed.* **1998**, *36*, 3101.

(17) Hanley, K. J.; Lodge, T. P.; Huang, C.-I. *Macromolecules* **2000**, *33*, 5918.

(18) Lodge, T. P.; Pudil, B.; Hanley, K. J. *Macromolecules* **2002**, *33*, 5918.

(19) Lodge, T. P.; Hanley, K. J.; Pudil, B.; Alahapperuma, V. *Macromolecules* **2003**, *36*, 816.

(20) Bang, J.; Lodge, T. P.; Wang, X.; Brinker, K. L.; Burghardt, W. R. *Phys. Rev. Lett.* **2002**, *89*, 215505.

(21) McConnell, G. A.; Gast, A. P.; Huang, J. S.; Smith, S. D. *Phys. Rev. Lett.* **1993**, *71*, 2102.

(22) McConnell, G. A.; Lin, M. Y.; Gast, A. P. *Macromolecules* **1995**, *28*, 6754.

(23) Halperin, A.; Tirrell, M.; Lodge, T. P. *Adv. Polym. Sci.* **1992**, *100*, 33.

(24) Hamley, I. W.; Pople, J. A.; Diat, O. *Colloid Polym. Sci.* **1998**, *276*, 446.

(25) Nishiyama, Z. *Martensitic Transformation*; Academic Press: New York, 1978.

(26) Olsen, G. H.; Jesser, W. A. *Acta Metall.* **1971**, *19*, 1009.

(27) Olsen, G. H.; Jesser, W. A. *Acta Metall.* **1971**, *19*, 1299.

(28) Shimizu, K.; Nishiyama, Z. *Metall. Trans.* **1972**, *3*, 1055.

(29) Bassett, W. A.; Huang, E. *Science* **1987**, *238*, 780.

(30) Wentzcovitch, R. M.; Cohen, M. L. *Phys. Rev. B* **1988**, *37*, 5571.

(31) Wada, M.; Uda, S.; Kato, M. *Philos. Mag. A* **1989**, *59*, 31.

(32) Wentzcovitch, R. M.; Krakauer, H. *Phys. Rev. B* **1990**, *42*, 4563.

(33) Wentzcovitch, R. M. *Phys. Rev. B* **1994**, *50*, 10358.

(34) Wang, C.-Y.; Lodge, T. P. *Macromolecules* **2002**, *35*, 6997.

(35) Caputo, F. E.; Ph.D. Thesis, Northwestern University, 2002.

(36) Caputo, F. E.; Burghardt, W. R.; Krishnan, K.; Bates, F. S.; Lodge, T. P. *Phys. Rev. E* **2002**, *66*, 041401.

(37) Koppi, K. A.; Tirrell, M.; Bates, F. S.; Almdal, K.; Colby, R. H. *J. Phys. Fr. II* **1992**, *2*, 1941.

(38) Fredrickson, G. H.; Leibler, L. *Macromolecules* **1989**, *22*, 1238.

(39) Hoover, W. G.; Young, D. A.; Grover, R. *J. Chem. Phys.* **1972**, *56*, 2207.

(40) Mendelson, S. *Scr. Metall.* **1977**, *11*, 375.

(41) Alexander, S.; McTague, J. *Phys. Rev. Lett.* **1978**, *41*, 702.

(42) Ziherl, P.; Kamien, R. D. *Phys. Rev. Lett.* **2000**, *85*, 3528.

Close-Packed and BCC Lattices

J. Phys. Chem. B, Vol. 107, No. 44, 2003 **12081**

(43) Ziherl, P.; Kamien, R. D. *J. Phys. Chem. B* **2001**, *105*, 10147.

(44) Chen, L. B.; Zukoski, C. F.; Ackerson, B. J.; Hanley, H. J. M.; Straty, G. C.; Barker, J.; Glinka, C. J. *Phys. Rev. Lett.* **1992**, *69*, 688.

(45) Diat, O.; Porte, G.; Berret, J.-F. *Phys. Rev. B* **1996**, *54*, 869.

(46) Molino, F. R.; Berret, J.-F.; Porte, G.; Diat, O.; Lindner, P. *Eur. Phys. J. B* **1998**, *3*, 59.

(47) Hamley, I. W.; Pople, J. A.; Fairclough, J. P. A.; Terrill, N. J.; Ryan, A. J.; Booth, C.; Yu, G.-E.; Diat, O.; Almdal, K.; Mortensen, K.; Vigild, M. *J. Chem. Phys.* **1998**, *108*, 6929.

(48) Hamley, I. W.; Pople, J. A.; Gleeson, A. J.; Komanschek, B. U.; Towns-Andrews, E. *J. Appl. Crystallogr.* **1998**, *31*, 881.

(49) Vigild, M. E.; Almdal, K.; Mortensen, K.; Hamley, I. W.; Fairclough, J. P. A.; Ryan, A. J. *Macromolecules* **1998**, *31*, 5702.

(50) Fairclough, J. P. A.; Ryan, A. J.; Hamley, I. W.; Li, H.; Yu, G.-E.; Booth, C. *Macromolecules* **1999**, *32*, 2058.

(51) Daniel, C.; Hamley, I. W.; Mingvanish, W.; Booth, C. *Macromolecules* **2000**, *33*, 2163.

(52) Daniel, C.; Hamley, I. W.; Wilhelm, M.; Mingvanish, W. *Rheol. Acta* **2001**, *40*, 39.

(53) Eiser, E.; Molino, F.; Porte, G.; Pithon, X. *Rheol. Acta* **2000**, *39*, 201.

(54) Eiser, E.; Molino, F.; Porte, G.; Diat, O. *Phys. Rev. B* **2000**, *61*, 6759.

(55) Hamley, I. W.; Daniel, C.; Mingvanish, W.; Mai, S.-M.; Booth, C.; Messe, L.; Ryan, A. J. *Langmuir* **2000**, *16*, 2508.

(56) Castelletto, V.; Hamley, I. W.; Holmqvist, P.; Rekatas, C.; Booth, C.; Grossmann, J. G. *Colloid Polym. Sci.* **2001**, *279*, 621.

(57) Hamley, I. W.; Castelletto, V.; Fundin, J.; Yang, Z.; Price, C.; Booth, C. *Langmuir* **2002**, *18*, 1051.

(58) Loose, W.; Ackerson, B. J. *J. Chem. Phys.* **1994**, *101*, 7211.

(59) Lai, C.; Russel, W. B.; Register, R. A. *Macromolecules* **2002**, *35*, 169.

(60) Williams, D. B.; Carter, C. B. *Transmission Electron Microscopy*; Plenum Press: New York, 1996.

(61) Bruce, L. A.; Jaeger, H. *Philos. Mag. A* **1978**, *37*, 337.

(62) Bruce, L. A.; Jaeger, H. *Philos. Mag. A* **1979**, *40*, 97.

(63) Ryder, P. L.; Pitsch, W. *Acta Metall.* **1966**, *14*, 1437.

(64) Ryder, P. L.; Pitsch, W.; Mehl, R. F. *Acta Metall.* **1967**, *15*, 1431.

(65) Dahmen, U. *Acta Metall.* **1982**, *30*, 63.

(66) Gotoh, Y.; Aral, I. *Jpn. J. Appl. Phys.* **1986**, *25*, L583.

(67) Headley, T. J.; Brooks, J. A. *Metall. Mater. Trans. A* **2002**, *33A*, 5.